

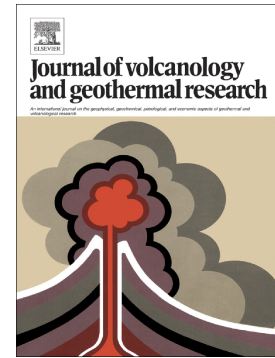
This is the Post-print version of the following article: *Jaime G. Pacheco-Hoyos, Gerardo J. Aguirre-Díaz, Pablo Dávila-Harris, Boiling-over dense pyroclastic density currents during the formation of the ~100km<sup>3</sup> Huichapan ignimbrite in Central Mexico: Stratigraphic and lithofacies analysis, Journal of Volcanology and Geothermal Research, Volume 349, 2018, Pages 268-282,* which has been published in final form at: [10.1016/j.jvolgeores.2017.11.007](https://doi.org/10.1016/j.jvolgeores.2017.11.007)

© 2018. This manuscript version is made available under the Creative Commons Attribution-NonCommercial-NoDerivatives 4.0 International (CC BY-NC-ND 4.0) license <http://creativecommons.org/licenses/by-nc-nd/4.0/>

## Accepted Manuscript

Boiling-over dense pyroclastic density currents during the formation of the ~100km<sup>3</sup> Huichapan ignimbrite in Central Mexico: Stratigraphic and lithofacies analysis

Jaime G. Pacheco-Hoyos, Gerardo J. Aguirre-Díaz, Pablo Dávila-Harris



PII: S0377-0273(17)30093-8  
DOI: doi:[10.1016/j.jvolgeores.2017.11.007](https://doi.org/10.1016/j.jvolgeores.2017.11.007)  
Reference: VOLGEO 6234

To appear in: *Journal of Volcanology and Geothermal Research*

Received date: 4 February 2017  
Revised date: 9 November 2017  
Accepted date: 9 November 2017

Please cite this article as: Jaime G. Pacheco-Hoyos, Gerardo J. Aguirre-Díaz, Pablo Dávila-Harris, Boiling-over dense pyroclastic density currents during the formation of the ~100km<sup>3</sup> Huichapan ignimbrite in Central Mexico: Stratigraphic and lithofacies analysis. The address for the corresponding author was captured as affiliation for all authors. Please check if appropriate. *Volgeo*(2017), doi:[10.1016/j.jvolgeores.2017.11.007](https://doi.org/10.1016/j.jvolgeores.2017.11.007)

This is a PDF file of an unedited manuscript that has been accepted for publication. As a service to our customers we are providing this early version of the manuscript. The manuscript will undergo copyediting, typesetting, and review of the resulting proof before it is published in its final form. Please note that during the production process errors may be discovered which could affect the content, and all legal disclaimers that apply to the journal pertain.

**Boiling-over dense pyroclastic density currents during the formation of the ~100km<sup>3</sup> Huichapan ignimbrite in Central Mexico: stratigraphic and lithofacies analysis**

**Pacheco-Hoyos, Jaime G.**<sup>1</sup>

**\*Aguirre-Díaz, Gerardo J.**<sup>2</sup>

**Dávila-Harris, Pablo**<sup>3</sup>

<sup>1</sup>Posgrado en Ciencias de la Tierra, Centro de Geociencias, Universidad Nacional Autónoma de México, Campus Juriquilla, Querétaro, Qro., 76230, México. geojgph@gmail.com

<sup>2</sup>Centro de Geociencias, Universidad Nacional Autónoma de México, Campus Juriquilla, Querétaro, Qro., 76230, México. E-mail: ger@geociencias.unam.mx

<sup>3</sup>IPICYT, División de Geociencias Aplicadas, San Luis Potosí, México; E-mail: pablo.davila@ipicyt.edu.mx.

\*Corresponding author

**Abstract**

A lithofacies analysis of the Huichapan ignimbrite has been undertaken to evaluate its depositional history from large pyroclastic density currents. The Huichapan ignimbrite is a massive ignimbrite sheet with a maximum runout of at least 55 km and thickness variations between 6 and 80 meters. The lower portion of the Huichapan ignimbrite consists of a large plateau [ $\sim 100 \text{ km}^3$ ;  $69 \text{ km}^3$  as dense-rock equivalent (DRE)] of massive ignimbrites with welding variations from densely welded to partly welded, devitrification, and high-temperature vapor-phase alteration. The lower part grades laterally to moderately welded and non-devitrified ignimbrites. These variations are interpreted as the sedimentation of density-stratified pyroclastic density currents erupted as boiling-over pulses from the Huichapan-Donguinyó caldera complex at a continuous rate, supporting deposition by quasi-steady progressive aggradation of sustained and hot currents. To the

north of the caldera, the lower portion of the ignimbrite consists of a small plateau (<10 km<sup>3</sup>) in which the densely welded and devitrified lithofacies are absent. Our interpretation is that the pyroclastic density currents flowed late to the north of the caldera and formed a smaller ignimbrite plateau with respect to the western one. This northern ignimbrite plateau cooled faster than the western ignimbrite plateau. Deposition-induced topographic modifications suggest that topographic obstacles, such as remnants of older volcanoes, may have promoted the deviation of the density currents to the north. The upper portion of the ignimbrite is composed of extensive, massive, coarse clast-rich, non-devitrified, and non-welded ignimbrites with abundant fines-poor pipes. This upper part was deposited from largely sustained and rapidly aggrading high-concentration currents in a near end-member, fluid escape-dominated flow boundary zone. The absence of welding in the upper portion may record pyroclastic density currents cooling during the formation of a relatively high pyroclastic fountain at the vent. We have established a depositional model for the Huichapan ignimbrite that explains the differences between the western and northern plateaus. The Huichapan ignimbrite was formed during a large caldera-forming eruption with concentrated pyroclastic fountains. High mass-flow rate was maintained for long periods, promoting the mobility of the pyroclastic density currents.

**Keywords:** Ignimbrite, welding, boiling-over currents, sustained eruptions, pyroclastic currents processes, Trans-Mexican Volcanic Belt.

## 1. Introduction

Pyroclastic density currents (PDCs) are devastating, gravity-driven gas-solid dispersions generated during explosive volcanic eruptions. They are a major geological hazard about which volcanologists need to understand their formation and emplacement processes (Sulpizio et al., 2014; Dufek, 2015; Neri et al., 2015). Ignimbrite geology can be interpreted through field studies of the deposits (e.g., Cas and Wright, 1987; Branney and Kokelaar, 2002; Brown et al., 2007), as well as with experiments and numerical modeling (e.g., Andrews and Manga 2012; Bursik and Woods, 1996; Neri and Macedonio, 1996; Darteville et al., 2004; Dufek et al., 2009; Rowley et al., 2014). Numerical and

experimental studies facilitate quantitative analysis of the governing processes during PDC sedimentation. Nevertheless, geological studies are the basis for understanding the processes reproduced during quantitative modeling and experiments (Kokelaar and Branney, 1996; Gottsman and Marti, 2008; Sulpizio et al., 2014). Recently, PDC deposits have been classified into those originated during small volume and large volume volcanic eruptions (Brown and Andrews, 2015). Every year, small-volume PDCs are common worldwide, whereas the largest PDC-forming eruptions that may devastate large areas have not yet been historically attested (Self, 2006). Because of this, deposit analysis is the main source of information for understanding the emplacement mechanism of large PDC systems. Studies of the PDC deposit architecture have been undertaken for moderately (several tens of km<sup>3</sup>; e.g., Allen, 2001; Brown and Branney, 2004, 2013) to very large volume ignimbrites (several hundreds of km<sup>3</sup>; e.g., Wilson, 2001; Wilson and Hildreth, 1997, 2003; Cas et al., 2011) in order to understand the emplacement processes of PDCs during large volcanic eruptions. The Huichapan ignimbrite is a Pliocene, nearly massive out-flow bed with a volume of about 100 km<sup>3</sup>. It is located in central Mexico, within the Trans-Mexican Volcanic Belt (TMVB). In this work, we present a lithofacies analysis of the Huichapan ignimbrite and describe its regional and local variations in welding, devitrification, vapor-phase alteration, granulometry, lithology and primary sedimentary structures. We provide an interpretation of the Huichapan ignimbrite's eruption and emplacement mechanisms.

### *1.1. Deposition of sustained pyroclastic density currents*

The progressive aggradation model is particularly useful for interpreting the deposition processes of sustained currents, in which runout distance, flow direction, velocity, concentration, flow capacity, and flow rheology evolves through time and space (e.g., Branney and Kokelaar, 1992, 2002). A pioneering view of the progressive aggradation model was presented by Fisher (1966), who proposed that the deposition of PDCs is an incremental process. Fisher (1966) suggests that the deposits' characteristics reflect processes within a boundary layer at the lower portion of PDCs. Lowe (1988) explains the sedimentation of gravity currents in terms of variable shearing rate, concentration, and suspended-load fallout rate. Similar ideas are further developed by Branney and Kokelaar

(2002) who propose the flow-boundary zone (FBZ) concept to explain the lithofacies variations within ignimbrites deposited via progressive aggradation. The FBZ includes the lowermost part of a current and uppermost part of a deposit in which a continuum of variables such as shear rate, concentration, and deposition rate, determine many of the deposit characteristics. The FBZ concept of Branney and Kokelaar (2002) makes special note of the role of the gaseous phase during the formation of PDC deposits. The FBZ types include four intergradational end-members (direct fallout-, traction-, fluid escape-, and granular flow-dominated). Each type of flow-boundary zone is characterized by a specific velocity, concentration, shear rate, and deposition rate. There is a continuum between all the previously mentioned parameters and, consequently, between the four end-member types of FBZ. During the assembly of an ignimbrite sheet FBZ processes may evolve in both time and space.

## 2. Geological setting

The TMVB is a Middle Miocene-Quaternary continental arc located in central Mexico, which is a highly populated area where many major cities are located. Calderas are common in the TMVB (e.g., Aguirre-Díaz, 1996; Aguirre-Díaz and McDowell, 1999; Aguirre-Díaz and López-Martínez, 2001, 2009; Ferriz and Mahood, 1984; Mahood, 1980). Despite the presence of caldera volcanoes, there are few studies on the physical volcanology of the relatively large ignimbrites in the TMVB (on the order of tens of cubic kilometers; e.g., Wright, 1981; Carrasco-Nuñez and Branney, 2005). The Donguinyó-Huichapan caldera complex (DHCC) is a 5-4 Ma eruptive center that comprises two nested trap-door calderas (Aguirre-Díaz and López-Martínez., 2009). The youngest one is the Huichapan caldera, from which the Huichapan ignimbrite erupted (Fig. 1). General stratigraphy, geochemical, and geochronological data, and differences between the Huichapan ignimbrite and other caldera-derived ignimbrites in the study area were presented by Aguirre-Díaz and López-Martínez (2009). The Huichapan ignimbrite is a calc-alkaline rhyolite with an  $^{40}\text{Ar}$ - $^{39}\text{Ar}$  age of 4.2 Ma (Aguirre-Díaz and López-Martínez, 2009).

Figure 1.

### Terminology, samples, and methods.

We use the term ignimbrite for the deposit of a dense pyroclastic density current rich in pumice and pumiceous ash shards (Freundt et al., 2000). The terms moderate-grade and high-grade ignimbrites follow the usage of Branney and Kokelar (1992). We use the welding rank scheme of Quane and Russell (2005); a rank 1 ignimbrite lacks welding and a rank 6 ignimbrite is a densely welded, glassy rock. We assign welding rank following the petrographic features presented by Quane and Russell (2005). We use the term surge for a peak in a parameter (e.g., velocity, capacity, shear rate) followed by a decrease in the same parameter. The term surge is used taking a fixed location as reference. Architecture refers to the overall structure and geometry of a deposit, including the 3D lithofacies arrangement (e.g., Miall, 1985; Branney and Kokelar, 2002). We use a lithofacies code (e.g., Miall, 1978; Sohn and Chough, 1989; Branney and Kokelar, 2002) for the systematization of the description of Huichapan ignimbrite's lithofacies (Table 1). The information for the stratigraphic scheme and physical volcanology interpretations is provided by the lithofacies code. The granulometry scale follows the usage of Fisher (1961). Thirty-four (34) representative logs are included in this work. In addition, the Huichapan ignimbrite has been studied at several other localities for stratigraphic correlation purposes. Systematic measurements of the largest observed lithic clast (~360 measurements) were taken in well exposed locations to identify local and regional grading patterns. Componentry percentages of the deposits were based on semiquantitative field estimations.

Forty-seven (47) thin-sections were described in detail to characterize the componentry and textures of Huichapan ignimbrite's lithofacies. Powder X-ray diffraction (XRD) analyses were performed at Centro de Geociencias (CGEO) of the Universidad Nacional Autónoma de México (UNAM) to identify vapor-phase minerals. Bulk samples were ground in fine powder < 100 mesh using an agate mill. Analyses were performed in a Rigaku Miniflex diffractometer with Cu – K $\alpha$  radiation. Operating conditions of the equipment were 30 kV and 15 mA. Step scan was 0.02°/2 $\theta$  at 1°/min. Identification of mineral phases was completed by comparing diffraction peak positions and intensity values with reference patterns in the ICDD PDF2 powder diffraction file. Analyzed XRD samples were taken from sites 20 and 4.

Table 1.

### 3. Results.

#### 3.1. Overview of the Huichapan ignimbrite

The Huichapan ignimbrite is a large and almost totally massive out-flow bed, classified as a moderate grade ignimbrite and welding grading from totally non-welded to densely welded (ranks 1 to near 6). The Huichapan ignimbrite grades from non-devitrified to strongly devitrified, and from fines-rich tuff layers to pumice-rich breccia facies, with lateral and vertical changes. In order to simplify the architecture of the Huichapan ignimbrite we propose to subdivide it into two main stratigraphic units: A Lower Huichapan ignimbrite member (LHI) and an Upper Huichapan ignimbrite member (UHI; Fig. 2). In this section, we define the overall characteristics of the Huichapan ignimbrite. Then, we focus on the lithofacies and interpretation of the LHI and UHI members.

Figure 2.

#### 3.2. Distribution, thickness, volume and componentry.

The Huichapan ignimbrite is crystal-poor (<5 vol. % in most bulk ignimbrite samples). Minerals include quartz, sanidine and plagioclase. Only quartz and sanidine have been observed within fiamme and pumice clasts. Pumice clasts include frothy pumices, tube pumices, transitional pumice between frothy and tube, and kink-banded tube pumices (Fig. 2). Lithic clasts include obsidian, vesicular basalt, chloritized andesite, eutaxitic ignimbrite, scoria, and dark-colored afanitic andesite. The latter is the most common lithic clasts, which sometimes is red in color due to oxidation. The afanitic andesite is the only lithic clast type found through the whole ignimbrite, the other lithic clast types appear sporadically at individual sites. Thicknesses vary from 6 meters to 80 meters in some composite sections and the runout distance of the ignimbrite is at least 55 km. The Huichapan ignimbrite has a minimum coverage of 2460 km<sup>2</sup> with a minimum volume of 108 km<sup>3</sup> just for the out-flow ignimbrite without considering the co-ignimbrite ash and the intra-caldera ignimbrite (see Supplementary Material 1 for volume estimation procedure). To calculate the DRE, we considered the mean density of a typical poorly welded ignimbrite as 1500 kg m<sup>-3</sup> (Folkes et al., 2011) and a dense rock equivalent for rhyolitic ignimbrites of 2349 kg m<sup>-3</sup> (Leshner and Spera, 2015; typical rhyolite at the solidus conditions of 900°C and 1 bar). The result is that the Huichapan ignimbrite yields a



minimum DRE volume of 69 km<sup>3</sup>. The Huichapan ignimbrite rests on horizontal surfaces in sites where the base was observed, but it ponded against relatively high mountains, such as older volcanoes and domes, which are partially covered by the ignimbrite at the medial and distal facies. Apparently, most of the Huichapan ignimbrite is a large, horizontally continuous sheet, which significantly leveled the topography. The ignimbrite forms a practically flat upper surface, with general slopes of less than 1° outwards from the vent (the DHCC), with ravines and canyons cutting through it, in places forming smooth hills between ravines due to erosion. The northern plateau is flat with a horizontal top and cliff-forming eroded borders.

#### 4.3. *Underlying units.*

The Huichapan ignimbrite overlies paleosols, fluvio-lacustrine deposits, older volcanic rocks, including reworked pyroclastic units, older ignimbrites, such as the Donguinyó tuff, San Joaquín tuff and Amealco tuff, and andesitic lavas of older volcanoes, such as Taxbathá (9.0 Ma) to the north, and Ñadó (Miocene) to the west, and 7.5 Ma andesites at the northern outcrops nearby San Francisco (Aguirre-Díaz and López-Martínez, 2009). It also ponded against the Sierra Los Caballos rhyolitic-dacitic, Miocene domes to the NW (Aguirre-Díaz and López-Hernández, 2009). The base of the Huichapan ignimbrite has been observed over a large area in downcurrent sites of both the western and northern plateaus (sites 3, 4, 10, 14, 26-30; Fig. 1), but is not exposed at proximal or medial sites. There is no evidence of an extensive fall deposit immediately at the base of the ignimbrite. Fall units have been observed at the study area, but are not related to the Huichapan ignimbrite as they appear separated by paleosols and fluvio-lacustrine deposits. Well-sorted, pumice-rich, 1-2 cm thick, coarse ash-rich tuffs layers have been observed at the base of the Huichapan ignimbrite at some sites (4, 14, 28-30; Fig. 1). Those layers are laterally discontinuous, rich in rounded and sub-rounded pumice and do not show systematic thickness or granulometric variations in relation to the distance from the vent. We interpret those tuff layers as pumiceous material embedded at lower portions of the PDCs during the emplacement of the Huichapan ignimbrite. Rounding of pumice clast suggest abrasion during deposition of the PDCs (e.g., Manga et al., 2011).

#### 4.4. *Lower Huichapan ignimbrite (LHI)*

The lower portion of the Huichapan ignimbrite is a monotonous, structureless, poorly sorted deposit, with mLT and emLT (Table 1) as the main lithofacies. The LHI ranges from non-welded (rank 1) to densely welded (between ranks 5-6), and from non-devitrified to strongly devitrified, with common occurrence of vapor-phase altered lithofacies. Fines-poor pipes are almost totally absent within the LHI, but cooling joints are widespread and often very well developed within the LHI. Both pumice-rich lithofacies and block-size pumices are rare with the largest pumice clast reaching up to 12 cm. Fine-grained layers (mT, mT (ip), dbT) are common at the base of the LHI. In some sites, a gradual increase in the size of both lithic and pumice clasts are recorded at the top of LHI outcrops (e.g., sites 10-12, 30, and 33; Fig. 1). The 100 largest observed lithic clasts in the LHI average 2.01 cm ( $1 \sigma = 1.13$ ).

#### 4.4.1. Lower Huichapan ignimbrite's zones 1, 2, and 3.

To describe the zonal variations in welding, devitrification, and vapor-phase alteration within the LHI we introduce the zones 1, 2, and 3 (Fig. 2), which are described below. These zones are characterized by eutaxitic massive lapilli-tuff (emLT), eutaxitic massive lapilli-tuff vitrophyre (vemLT), devitrified eutaxitic massive lapilli-tuff (devemLT), and vapor-phase altered massive lapilli-tuff (vapmLT). Cooling joints are common features in zones 1, 2, and 3 (Fig. 3), but are not developed throughout the LHI; instead, they become less well-developed away from the vent, as shown in Fig. 1 and Fig. 2. The complete description and detailed analysis of the zones is summarized in Table 2. Textural variations between these three zones are shown as photomicrographs in Fig. 4. Zones 1, 2, and 3 within the LHI are widespread and follow the same vertical pattern through several hundred km<sup>2</sup> (Figs. 1 and 2).

Table 2.

Figure 3.

Figure 4.

#### 4.4.2. Western Lower Huichapan ignimbrite

The LHI in the west of the study area is composed of widespread, monotonous, structureless, and poorly-graded deposits (Fig. 5). However, a gradual increase in the size of both pumice and lithic clasts was observed at sites 10-12 (Fig. 1). Lithofacies are composed of mLT and emLT, sometimes with grain fabric, grading laterally into the LHI's zones 1, 2, and 3, which also are structureless and poorly graded deposits (Figs. 2 and 5).

Figure 5.

#### 4.4.3. Northern Lower Huichapan ignimbrite

The LHI in the north is predominantly composed of massive lapilli-tuff lithofacies sometimes with eutaxitic texture (mLT, emLT). In the north, the ignimbrite vertically and laterally passes from non-graded, to inversely graded, to normally graded, for both lithic and pumice clasts. Several lithofacies, such as basal fines-rich bases (mT) or pumice-rich horizons (pmBr, pmLT) are laterally inconsistent between sites. A detailed analysis of the northern LHI is presented in Table 3 and logs of sections in Fig. 6. Zones 1, 2, and 3 are not present in the northern exposures. Field photographs of representative lithofacies are shown in Fig. 7.

Table 3.

Figure 6.

Figure 7.

#### 4.5. Upper Huichapan ignimbrite (UHI)

The UHI is totally non-welded (rank 1 ignimbrite) and non-devitrified throughout its extent; the deposit is almost totally massive and poorly sorted. Well-developed, fines-poor, lithic-rich degasification pipes are common in all sites of the UHI (Fig. 8a), with the degasification pipes ranging from a few centimeters to several meters long (up to 5 m). Cooling joints are absent within the UHI. Block-size pumice is common in all sites of the UHI with the largest pumice clast between 0.65 -1 m; this is significantly larger than the pumice in the LHI, which rarely reach 12 cm. The 100 largest observed lithic clasts in the UHI average 3.13 cm ( $1 \sigma = 1.57$ ), which is 1.12 cm larger than those in the LHI. Because of this, the Huichapan ignimbrite has an inverse grading of both lithic and pumice clasts,

being the pumice grading of the coarse-tail type. Within the UHI outcrops, pumices are inversely graded and lithics are normally or inversely graded (see sites 6, 17, and 25 in Figs. 2 and 6). The lithofacies that best represents the UHI is pmLT (pip), although there is a continuum between the mLT – pmLT - pmBr lithofacies (Fig. 8b, c). Pumice-rich massive breccias (pmBr) are observed locally in the UHI in sites with inverse coarse-tail grading of pumice (e.g., site 6, Fig. 2), or as discontinuous pumice concentration zones lenses. Tube pumice is nearly 80% of the total pumice population in the UHI. The transition between the LHI and the UHI is gradual, as revealed by the coarsening- upward succession observed at upper zones of the LHI (e.g., sites 10-12, 29, 30, and 32, Fig. 1). Although the contact between the LHI and UHI is very poorly exposed, in ravines located 8 km to the west of site 15 there is a gradual transition of features between the LHI and UHI without a paleosol between them.

Figure 8.

## 5. Discussion

### 5.1. Huichapan ignimbrite as a single depositional unit.

Since both the LHI and UHI are composed of the same lithic and pumice clasts, and there are gradual transitions between both members, we interpret the Huichapan ignimbrite as a single depositional ignimbrite unit formed by an uninterrupted, but pulsating eruption. The differences in granulometry may reflect variations in the size of both lithic and pumice clasts erupted at the vent. Despite the complexity of the individual grading patterns at each studied site, the whole ignimbrite has an inverse coarse-tail grading of both lithic and pumice clast, indicating that the size of the clast increased as the eruption progressed. A simplified section of the Huichapan ignimbrite is shown in Fig. 9.

Figure 9.

### 5.2. Deposition of western LHI.

To the west, the LHI marks deposition from quasi-steady, depletive, density-stratified high-concentration currents in a fluid-escape dominated FBZ (e.g., Kneller and Branney, 1995). A gradual increase in current competence is shown by the coarsening-upward

successions at some sites, interpreted to record a transition into the more coarse-grained UHI. This is in agreement with the “steady deposition regime” described by Sulpizio et al (2014), and we consider the LHI to be an example of a steady thickening of the deposits with time. Grain fabric records transitions to a granular-flow-dominated FBZ.

### *5.3. Deposition of northern LHI.*

The northern LHI's architecture is the result of dense pyroclastic current deposition and the evolution of FBZ processes in time and space. Several specific depositional histories have been identified in the northern LHI. These include: 1) quasi-steady currents (e.g., site 33); 2) waxing currents (e.g., site 27); 3) waning currents (e.g., site 26); 4) surging currents (e.g., site 28); and 5) waxing then quasi-steady currents (e.g., site 34). The most common depositional regime is quasi-steady progressive aggradation of density-stratified, high-concentration currents in a fluid escape-dominated FBZ.

### *5.4. Deposition of the UHI.*

The widespread abundance of large pumice lumps indicates that the UHI was deposited from pumice-rich currents; however, particularly pumice-rich portions within the UHI (e.g., pmBr) may indicate some influence of segregation processes (Table 4). Fines-poor pipes within the UHI may have formed because of the effect of ascending gases from the LHI, but we interpret this as a rapid progressive aggradation from largely sustained currents in a near-end member fluid escape-dominated FBZ. In other words, a rapid vertical aggradation with almost zero lateral shearing, promoting highly effective fluid (gas and fine ash) vertical channeling within the deposits because of the effect of processes such as hindered settling, deposition and compaction (e.g., Druitt, 1995; Branney and Kokelaar, 2002; Brown and Andrews, 2015). Inverse to normal grading of lithic clasts between sites indicates that currents forming UHI were not uniform, changing from waxing to waning flow competence (respectively) in time and space.

Table 4.

### *5.5. Thermal interpretation of the Huichapan ignimbrite.*

In order to create the strong welding and devitrification textures observed in portions of the LHI (see Table 2), the PDCs are likely to have been hotter than the glass transition temperature of a typical calc-alkaline rhyolite, between 600-750°C (Druitt, 1998). For the LHI we interpret rapid and uninterrupted deposition of extensive and relatively hotter PDCs whose deposits cooled as a simple cooling unit (*sensu* Smith, 1960). The abundance of lithofacies interpreted as being formed by deposits remaining at temperatures exceeding the glass transition temperature for long periods of time (e.g., vemLT, devemLT, vapmLT), suggest that the LHI's forming PDCs may have been particularly hot. The fact that zones 1, 2, and 3 fade out laterally within the LHI is because of higher degrees of cooling as the sheet thins from the source (more prone to vertical heat loss), and there is higher lateral heat loss in distal margins of the sheet. This differs from the very high-grade ignimbrites that may be welded in distal margins of the ignimbrite sheet and/or in very thin deposits (e.g., Walker, 1983; Branney and Kokelaar, 1992). The UHI is totally non-welded and lacks high-temperature devitrification, which may be because the UHI was emplaced later during the eruption, after hotter LHI was emplaced, from material that reached higher over the vent and was already cool when it reached the ground. We thus propose that the UHI may have formed from a relatively high-height pyroclastic fountain, which promote cooling of the PDCs with ambient fluid and eventually lead to the formation of non-welded deposits (e.g., Sparks et al., 1978).

#### 5.6. Eruptive model.

The following eruptive model is proposed to explain the spatial distribution of the LHI and UHI members of the Huichapan ignimbrite, including the distribution of the zones 1, 2, and 3 within the former (Fig. 10).

Figure 10.

##### 5.6.1. Phase 1. Formation of LHI (Fig.10a).

In the conceptual model presented here, the eruption starts with the formation of low PDCs boiling-over the vent, which are relatively hotter and composed of density-stratified high-concentration currents. These currents lead to the formation of the massive

deposits. Deposition and lateral movement of the PDCs were occurring at the same time, so it could be expected that the maximum runout distance of the currents continuously increased with time. Both basal high-particle concentrations in the PDCs and the long runout distances were maintained because of the continuous supply of dense currents at the vent. This kind of eruption is predicted by the model of Roche et al. (2016), and the deposits of such kinds of events are expected to be highly massive because of high particle concentration and turbulence inhibition towards the FBZ. The deposits are also expected to show evidence of hot emplacement, such as welding and high-temperature devitrification, because slow currents have little air entrainment during emplacement (e.g., Bursik and Woods, 1996). As previously discussed, the granulometry of the erupted granular dispersions may be an important factor controlling the height of the pyroclastic fountains (Dufek et al., 2012). The PDCs could be described in terms of “forced convection-dominated currents” (Doronzo, 2012), which are currents that are not dominated by their own inertia, but have the tendency to deposit and do not have the ability to surmount topographic barriers. Fig.10a illustrates the time when deposits extended to the west at the maximum runout distance that could be inferred from the most distal deposits preserved today (about 50 km), including the inferred Huichapan ignimbrite at the south. During phase 1, ongoing construction of a large ignimbrite plateau was taking place to the west.

#### 5.6.2. Phase 2. Formation of LHI continues (Fig. 10b).

During phase 2, the eruption continues with the formation of low, boiling-over, relatively hotter, density-stratified, high-concentration PDCs. The pre-Huichapan ignimbrite units to the NW, such as Miocene rhyolitic domes and mafic shield volcanoes, were large topographic obstacles during the emplacement of the Huichapan ignimbrite. These features are still preserved today as large topographic highs. During phase 2, the PDCs were erupted perpendicular to the caldera outline and were ponded against the obstacles. The PDCs were not dominated by their own inertia, and rather than surmounting the large topographic obstacles, thick deposits started to accumulate between them. As the ignimbrite became thicker, the topography was leveled and, eventually, it was easier for the PDCs to move to the north. During phase 2, deposition of the LHI was taking place at both the north and west of the study area. On the basis of this model, we can explain the

following observations. 1) The northern plateau is located in an area that is lateral to the western side of the caldera outline, so currents reached the north through the path between obstacles proposed in the model. 2) The deposits are thinner in the northern plateau than in the distal portions of the western plateau despite the fact that the former is closer to the vent and closer to the thickest preserved exposures of the Huichapan ignimbrite (Fig. 1). 3) The western ignimbrite plateau is larger than the northern ignimbrite plateau (106 km<sup>3</sup> and 20 km<sup>3</sup>, respectively) favoring this interpretation. 4) Zones 1, 2, and 3 fade out in the northern plateau whereas those zones could be traced laterally through a large area into the west (Figs. 1 and 2). Therefore, PDCs flowed north apparently late during LHI eruptions, forming a relatively smaller ignimbrite plateau.

#### 5.6.3. Phase 3. Formation of the UHI (Fig. 10c).

During phase 3, the eruption continued with the development of density-stratified high-concentration PDCs, leading to the formation of massive deposits. In phase 3, minor efficiency in the primary fragmentation mechanism (e.g., Kaminski and Jaupart, 1998) and/or minor degrees of “granular disruption” (breakup of particles due to collisions during ascent; Dufek et al., 2012), lead to the formation of pumice-rich PDCs with very coarse pumice clasts. Increased incorporation of lithics which could have been derived from the vent lead to the formation of PDCs with coarse and relatively abundant lithics in comparison to the PDCs of phases 1 and 2. However, it is unclear which lithics were derived from the vent, as most of them are andesitic clasts that could also have been derived from the paleo-surface as accidental lithics. There is an increase in lithics content during this phase which we interpret as vent erosion during eruption. During phase 3, the eruption transitionally evolves to a relatively high pyroclastic fountain. Evidence for this interpretation includes: 1) The non-welded nature of the UHI, which could be partially related to cooling during the formation of relatively high fountains (e.g., Sparks et al., 1978); 2) The large amount of tube pumice within the UHI may indicate the presence of stretched and long fissure vent conduits (Maissonueve et al., 2009). If this is the case, the stretched nature of the conduit may have favored the formation of a buoyant plume (e.g., Woods, 1998); 3) The UHI is rich in coarse-grained pumice, indicating deposition from coarse pumice-rich PDCs. In the model of Dufek et al (2012), fine-grained granular



dispersions are predicted to be more likely to be erupted in the form of low fountains whereas coarser-grained granular dispersions are predicted to be more likely to be erupted in the form of high fountains. The latter may have been the case for the UHI-forming PDCs. PDC fountains during phase 3 were probably relatively high boiling-over currents, high enough to promote air entrainment and cooling of the pyroclastic dispersions, preventing welding of the deposits, but not high enough to promote significant air entrainment and the formation of dilute currents.

*5.7. Comparison with other large ignimbrites and the continuum of processes during large ignimbrite-forming eruptions.*

Contrasting views on features interpreted as evidence of flow-unit boundaries have been published since the 1970s (e.g., Sparks, 1976; Cas and Wright, 1987; Wilson and Hildreth, 1997, 2002; Branney and Kokelaar, 2002; Brown and Branney, 2004). We follow the idea that the most reliable evidence (but not the only evidence) for identifying ignimbrite flow-unit boundaries are the presence of fall layers, reworked horizons, and/or water-rilled scour surfaces (Brown and Branney, 2004). We propose that the Huichapan ignimbrite was formed by continuous and uninterrupted deposition of density-stratified high-concentration PDCs, with pumice-concentration zones and complex grading patterns within the Huichapan ignimbrite reflecting changing FBZ conditions with time. Ignimbrites from the Aira caldera (Tsumaya and Ito ignimbrites) are homogenous and, in most exposures, do not show evidence of flow-unit boundaries (Aramaki, 1984). This lack of evidence of flow-unit boundaries is similar to the Huichapan ignimbrite, although intensity and relative abundance of welded facies is larger in the Huichapan ignimbrite than in ignimbrites from the Aira caldera. Deposits from the Campanian ignimbrite have also been interpreted to be formed from single sustained PDCs (Fedele et al., 2016). For the Ora ignimbrite, the strong welding and lack of evidence of an underlying extensive fall deposit was interpreted as an effect of the eruption by boiling-over of relatively hotter PDCs with no precursor buoyant plume (Willcock et al., 2013). Extensive welding and high-temperature devitrification within the LHI, as well as a lack of evidence of an underlying extensive fall deposit immediately before the ignimbrite, suggest that the model of Willcock et al. (2013) could also apply to the Huichapan ignimbrite. For the Cerro Galán

ignimbrite, Cas et al. (2011) interpreted the high emplacement temperature inferred from thermal remnant magnetization of lithic clasts (Lesti et al., 2011), and development of welding in proximal and medial regions as eruption of low boiling-over fountains that were never high. The evidence of high emplacement temperatures in the Huichapan ignimbrite is significant, as recorded by the zones 1, 2, and 3 of the LHI. Because of this, the Huichapan ignimbrite represents the result of hotter, low boiling-over, density-stratified high-concentration PDCs than the Cerro Galán ignimbrite. The most extreme case study of rhyolitic calc-alkaline ignimbrites formed by relatively hotter low boiling-over currents could be the Snake-River type high-grade ignimbrites of Yellowstone (Branney et al., 2008). For the Huichapan ignimbrite we propose that the pyroclastic fountains evolved from low boiling-over into fountains high enough to promote PDC cooling and the formation of the widespread and non-welded UHI. Largely sustained, slow, widespread, and far-travelled density-stratified high-concentration PDCs were inferred to form monotonous, massive, and poorly-sorted large ignimbrite sheets on the basis of deposit architecture (Cas et al., 2011). Recent models and experiments support these views (e.g., Doronzo, 2012; Roche et al., 2016) and the monotonous, massive and relatively large Huichapan ignimbrite fits well in this view. Large-volume ignimbrites with several interbedded fall deposits have been reported (e.g., Oraniu, Wilson, 2001; Bishop Tuff, Wilson and Hildreth, 1997, 2003), suggesting eruptive events with large production of PDCs but with simultaneous formation of fall deposits. For the Bishop Tuff, Wilson and Hildreth (1997, 2003) interpreted the existence of several flow units within the ignimbrite deposits; in contrast, the Cerro Galán ignimbrite is interpreted as a predominantly single massive unit (Cas et al., 2011), and this is also the case for the Huichapan ignimbrite. For large and mostly massive ignimbrite sheets, it seems that there is a continuum between ignimbrite forming-eruptions with cessation of PDCs and simultaneous formation of fall deposits, and ignimbrites that totally lack interbedded fall units; and there is also a continuum between ignimbrites composed of several flow units and single massive beds. The Bishop Tuff (Wilson and Hildreth, 1997, 2003) may represent an end member composed of ignimbrites largely coeval with fall units and the presence of several flow units within the ignimbrites, whereas cases such as the Cerro Galán ignimbrite (Cas et al., 2011) represent the end member of large, single massive depositional ignimbrite units. The

Huichapan ignimbrite, although not as large as the Cerro Galán ignimbrite, fits better with the second case.

#### *5.8. Facies analysis vs. facies models.*

The Huichapan ignimbrite was previously interpreted as an ignimbrite that shows agreement with the “standard ignimbrite flow unit” succession of Sparks et al. (1973) at most sites (Aguirre-Díaz and López-Martinez, 2009). From the new lithofacies analysis shown here, we reinterpret the Huichapan ignimbrite as a deposit that differs from the “standard ignimbrite flow unit” facies model of Sparks et al (1973) and modifications of this model (e.g., Sparks, 1976; Cas and Wright, 1987; Carey, 1991; Freundt et al., 2000). Some of the main reasons to support this new view are: 1) lateral inconsistency of lithofacies, sometimes interpreted as flow-unit boundaries (e.g., pumice concentration zones; Wilson and Hildreth, 1997); 2) complex grading patterns within the ignimbrite (including sites with inverse grading of pumices that pass laterally to sites with normal grading of pumice, see sites 26 and 27 in Fig. 6); 3) most sites do not show lithofacies association in agreement with idealized sequences. Sites that partially fit the lithofacies models’ sequences (e.g., site 26; Fig. 6) represent a particular case of deposition within a more complex evolving, largely sustained PDCs system. In addition, lithofacies associations that reflect waning flow conditions (site 26) grade laterally into sites indicative of waxing flow conditions (site 27). We follow the idea that lithofacies should not be grouped into idealized sequences and we prefer to interpret each particular lithofacies and lithofacies associations (as revealed by the application of the lithofacies code) in terms of flow dynamics and deposition processes (e.g., Branney and Kokelar., 2002; Sulpizio and Dellino., 2008; Postma and Cartigny., 2014).

## **6. Conclusions**

The lower (LHI) and upper (UHI) members of the Huichapan ignimbrite were formed by uninterrupted and largely sustained dense pyroclastic fountains that were maintained for the time that the eruption lasted. This induced the steady formation of density-stratified high-concentration PDCs, which maintained their mobility primarily because of the high mass flow rate. The lithofacies of the Huichapan ignimbrite are massive and were deposited

through fluid escape- and granular flow-dominated FBZ processes. Quasi-steady deposition was predominant, although several lithofacies associations within the Huichapan ignimbrite's architecture suggest non-uniform depositional histories through time and space. The large ignimbrite plateau of the LHI at the west contains significant proportions of densely welded, intensely devitrified, and vapor-phase altered lithofacies. These are inferred to record the emplacement of extensive, relatively hotter PDCs erupted as low boiling-over pyroclastic fountains. The densely welded, devitrified and vapor-phase altered lithofacies are absent in the northern portion of the LHI, which may be because deposition started late at that area, forming a relatively smaller plateau that was more rapidly cooled than the larger, western plateau. The non-welded nature of the UHI may record the transition to a relatively higher height, dense pyroclastic fountain in which the pyroclastic dispersion suffered cooling because of air entrainment. The UHI is richer and coarser grained in both lithic and pumice clasts than the LHI. The increase in pumice clasts may record less efficiency in the primary fragmentation mechanism and/or higher degrees of post-fragmentation disruption of the pyroclastic dispersion during ascent. The granulometry of the erupted granular dispersions, from fines-rich (LHI-forming PDCs) to coarse-grained (UHI-forming PDCs) may have altered the nature of the pyroclastic fountain processes from low to high fountains, respectively. The Huichapan ignimbrite provides a record of the eruptive processes and depositional mechanisms during the assembly of large ignimbrite sheets. This study helps to model the catastrophic emplacement of PDCs during caldera-forming eruptions.

### **Acknowledgments**

We thank Juan Tomás Vázquez and Marina Vega for laboratory support. We are grateful to Ivan Suñé and Dario Pedrazzi for their assistance in the field and valuable discussions at field sites. We kindly acknowledge editorial handling by Dr. James Gardner and the thorough revision by Dr. Marit Van Zalinge and an anonymous reviewer that strongly improved the quality of the manuscript. This work was supported by UNAM-PAEP student grant to the first author, and financed by UNAM-DGAPA grants PAPIIT-UNAM, IN-114606, PAPIIT-IN104615 and PAPIME-PE101816 to GJAD. JGPH was supported by a

CONACYT student scholarship. Dr. Aaron Martin is kindly acknowledged for reading through earlier versions of this manuscript.

### References cited

Aguirre-Díaz, G.J., 1996. Volcanic stratigraphy of the Amealco Caldera and vicinity, Central Mexican Volcanic Belt. *Revista Mexicana de Ciencias Geológicas* 13, 10-51.

Aguirre-Díaz, G.J., López-Martínez, M., 2001. The Amazcala caldera, Querétaro, México. *Geology and geochronology. Journal of Volcanology and Geothermal Research* 111, 203-218.

Aguirre-Díaz, G.J., López-Martínez, M., 2009. Geologic evolution of the Donguinyó-Huichapan caldera complex, central Mexican Volcanic Belt, Mexico. *Journal of Volcanology and Geothermal Research* 179,133-148.

Aguirre-Díaz, G.J., McDowell, F.W., 1999. Volcanic evolution of the Amealco caldera, central Mexico. *Geological Society of America Special Paper* 334, 1-14.

Allen, S.R., 2001. Reconstruction of a major caldera-forming eruption from pyroclastic deposit characteristics: Kos Plateau Tuff, eastern Aegean Sea. *Journal of Volcanology and Geothermal Research* 105, 141-162.

Andrews, B.J., Manga, M., 2012. Experimental study of turbulence, sedimentation, and coignimbrite mass partitioning in dilute pyroclastic density currents. *Journal of Volcanology and Geothermal Research* 225-226: 30-44.

Aramaki, S., 1984. Formation of the Aira Caldera, Southern Kyushu, ~ 22,000 years ago. *Journal of Geophysical Research* 89, 8485-8501.

Branney, M.J., Bonnicksen, B., Andrews, G.D.M., Ellis, B., Barry, T.L., McCurry, M., 2008. “Snake River (SR)-type” volcanism at the Yellowstone hotspot track: distinctive products from unusual, high-temperature silicic super-eruptions. *Bulletin of Volcanology* 70, 293-314.

Branney, M.J., Kokelaar, B.P., 1992. A reappraisal of ignimbrite emplacement: progressive aggradation and changes from particulate to non-particulate flow during emplacement of high-grade ignimbrite. *Bulletin of Volcanology* 54, 504-520.

Branney, M.J., Kokelaar, B.P., 2002. Pyroclastic density currents and the sedimentation of ignimbrites. *Geological Society of London Memoir* 27.

Brown, R.J., Andrews, G.D.M., 2015. Deposits of pyroclastic density currents. In: Sigurdsson, H., Houghton, B., Rymer, H., Stix, J., McNutt, S. (Eds), *The Encyclopedia of Volcanoes*, second edition, pp. 631-648.

Brown, R.J., Branney, M.J., 2004. Event-stratigraphy of a caldera-forming ignimbrite eruption on Tenerife: the 273 ka Poris Formation. *Bulletin of Volcanology* 66, 392-416.

Brown, R.J., Branney, M.J., 2013. Internal flow variations and diachronous sedimentation within extensive, sustained, density-stratified pyroclastic density currents flowing down gentle slopes, as revealed by the internal architectures of ignimbrites on Tenerife. *Bulletin of Volcanology* 75, 727.

Brown, R.J., Kokelaar, B.P., Branney, M.J., 2007. Widespread transport of pyroclastic density currents from large silicic tuff ring: the Glaramara tuff, Scafell caldera, English Lake District, UK. *Sedimentology* 54: 1163-1189.

Bursik, M.I., Woods, A.W., 1996. The dynamics and thermodynamics of large ash flows. *Bulletin of Volcanology* 58: 175-193.

Carey, S.N., 1991. Transport and deposition of tephra by pyroclastic flows and surges. *SEMP Special Publication* 45, 39-57.

Carrasco-Nuñez, G., Branney, M.J., 2005. Progressive assembly of a massive layer of ignimbrite with a normal-to-reverse compositional zoning: the Zaragoza ignimbrite of central Mexico. *Bulletin of Volcanology* 68, 3-20.

Cas, R.A.F., Wright, H.M.N., Folkes, C.B., Lesti, C., Porreca, M., Giordano, G., Viramonte, J.G., 2011. The flow dynamics of an extremely large volume pyroclastic flow, the 2.08-Ma Cerro Galán Ignimbrite, NW Argentina, and comparison with other flow types. *Bulletin of Volcanology* 73, 1583-1609.

Cas, R.A.F., Wright, J.V., 1987. *Volcanic Successions: Modern and Ancient*. Allen and Unwin.

Darteville, S., Rose, W.I., Stix, J., Kelfoun, K., Vallance, J.W., 2004. Numerical modeling of geophysical granular flows: 2. Computer simulations of Plinian clouds and flows and surges- *Geochemistry Geophysics Geosystems*. 5, Q08004, doi:10.1029/2003GC000637.

Doronzó, D.M., 2012. Two new end members of pyroclastic density currents: Forced convection-dominated and inertia-dominated. *Journal of Volcanology and Geothermal Research* 219-220, 87-91.

Druitt, T.H., 1995. Settling behaviour of concentrated dispersions and some volcanological applications. *Journal of Volcanology and Geothermal Research* 65, 27-39.

Druitt, T.H., 1998. Pyroclastic density currents. In: Gilbert, J.S., Sparks, R.S.J., (eds) *The physics of explosive volcanic eruptions*. Geological Society of London Special Publication no.145, p.145-182.

Dufek, J., 2015. The fluid mechanics of pyroclastic density currents. *Annual Review of Fluid Mechanics* 48: 459-85. doi: 10.1146/annurev-fluid-122414-034252.

Dufek, J., Manga, M., Patel, A., 2012. Granular disruption during explosive volcanic eruptions. *Nature Geoscience* 5, 561-564.

- Dufek, J., Wexler, J., Manga, M., 2009. Transport capacity of pyroclastic density currents: experiments and models of substrate-flow interaction. *Journal of Geophysical Research* 114: B11203, doi:10.1029/2008JB006216.
- Fedele, L., Scarpati, C., Sparice, D., Perrota, A., Laiena, F., 2016. A chemostratigraphic study of the Campanian Ignimbrite eruption (Campi Flegrei, Italy): Insights on magma chamber withdrawal and deposit accumulation as revealed by compositionally zones stratigraphic and facies framework. *Journal of Volcanology and Geothermal Research* 324, 105-117.
- Ferriz, H., Mahood, G.A., 1984. Eruption rates and compositional trends at Los Humeros volcanic center, Puebla, Mexico. *Journal of Geophysical Research* 89, 8511-8524.
- Fisher, R.V., 1961. Proposed classification of volcanoclastic sediments and rocks. *Geological Society of America Bulletin* 72, 1409-1414.
- Fisher, R.V., 1966. Mechanism of deposition from pyroclastic flows. *American Journal of Science* 264, 350-363.
- Fisher, R.V., 1979. Models for pyroclastic surges and pyroclastic flows. *Journal of Volcanology and Geothermal Research* 6, 305-318.
- Folkes, C.B., Wright, H.M., Cas, R.A.F., de Silva, S.L., Lesti, C., Viramonte, J.G., 2011. A re-appraisal of the stratigraphy and volcanology of the Cerro Galán volcanic system, NW Argentina. *Bulletin of Volcanology* 73, 1427-1454.
- Freundt, A., Wilson, C.J.N., Carey, S.N., 2000. Ignimbrites and block-and-ash flow deposits. In: Sigurdsson, H., et al. (Eds), *Encyclopedia of Volcanoes*, Academic Press, NY-London, pp. 581-599.
- Giordano, D., Nichols, A.R.L., Dingwell, D.B., 2005. Glass transition temperatures of natural hydrous melts: a relationship with shear viscosity and implications for the welding process. *Journal of Volcanology and Geothermal Research* 142, 105-118.
- Gottsmann, J. and Martí, J. (Eds.), 2008, *Caldera Volcanism: Analysis, Modelling and Response*. *Developments in Volcanology*, 10. Elsevier, *Caldera Volcanism: Analysis, Modelling and Response*. *Developments in Volcanology*, 10. Elsevier, 492 p.
- Kaminski, E., Jaupart, C., 1998. The size distribution of pyroclasts and the fragmentation sequence in explosive volcanic eruptions. *Journal of Geophysical Research* 103, 29759-29779.
- Kneller, B.C., Branney, M.J., 1995. Sustained high-density turbidity currents and the deposition of thick massive sands. *Sedimentology* 42, 607-616.
- Kokelaar, B.P., Branney, M.J., 1996. Comment on "On pyroclastic flow emplacement" by Maurizio Battaglia. *Journal of Geophysical Research* 101: 5653-5655.
- Legros, F., 2002. Can dispersive pressure cause inverse grading in grain flows? *Journal of Sedimentary Research* 72, 166-170.

- Leshner, C.E., Spera, C.E., 2015. Thermodynamic and transport properties of silicate melts and magma. In Sigurdsson (ed), *Encyclopedia of Volcanoes* (second edition). p. 113-141.
- Lesti, C., Porreca, M., Giordano, G., Mattei, M., Cas, R.A.F., Wright, H.M.N., Folkes, C.B., Viramonte, J., 2011. High-temperature emplacement of the Cerro Galán and Toconquis Group ignimbrites (Puna plateau, NW Argentina) determined by TRM analyses. *Bulletin of Volcanology* 73, 1535-1565.
- Lofgren, G., 1970. Experimental devitrification rate of rhyolite glass. *Geological Society of America Bulletin* 81, 553-560.
- Lofgren, G., 1971. Experimentally produced devitrification textures in natural rhyolitic glass. *Geological Society of America Bulletin* 82, 111-124.
- Lowe, D.R., 1988. Suspended-load fallout rate as an independent variable in the analysis of current structures. *Sedimentology* 35, 765-776.
- Mahood, G.A., 1980. Geologic evolution of a Pleistocene rhyolitic center – Sierra la Primavera, Jalisco, Mexico. *Journal of Volcanology and Geothermal Research* 8, 199-230.
- Maisonneuve, C.B., Bachmann, O., Burgisser, A., 2009. Characterization of juvenile pyroclast from the Kos Plateau Tuff (Aegean Arc): insights into the eruptive dynamics of a large rhyolitic eruption. *Bulletin of Volcanology* 71, 643-658.
- Manga, M., Patel, A., Dufek, J., 2011. Rounding of pumice clast during transport: field measurements and laboratory studies. *Bulletin of Volcanology* 73, 321-333.
- Miall, A.D., 1985. Architectural-element analysis: A new method of facies analysis applied to fluvial deposits. *Earth-Science Reviews* 22, 261-308.
- Miall, A.D., 1978. Lithofacies types and vertical profile models in braided river deposits: A summary. In: Miall, A.D. (Ed.), *Fluvial Sedimentology*. Canadian Society of Petroleum Geology Memoirs, 5, pp.597-604.
- Neri, A., Macedonio, G., 1996. Numerical simulation of collapsing volcanic columns with particles of two sizes. *Journal of Geophysical Research* 101: 8153-8174.
- Neri, A., Esposti Ongaro, T., Voight, B., Widiwijayanti, C., 2015. Pyroclastic density current hazards and risk. <http://dx.doi.org/10.1016/B978-0-12-396453-3.00005-8>.
- Postma, G., Cartigny, M.J.B., 2014. Supercritical and subcritical turbidity currents and their deposits – A synthesis. *Geology*, doi:10.1130/G35957.1.
- Quane, S.L., Russell, J.K., 2005. Ranking welding intensity in pyroclastic deposits. *Bulletin of Volcanology* 67, 129-143.
- Riehle, J.R., Miller, T.F., Bailey, R.A., 1995. Cooling, degassing and compaction of rhyolitic ash flow tuffs: A computational model. *Bulletin of Volcanology* 57, 319-336.



- Roche, O., Buesch, D.C., Valentine, G.A., 2016. Slow-moving and far-travelled dense pyroclastic flows during the Peach Spring super-eruption. *Nature Communications*, 7:10890, doi:10.1038/ncomms10890.
- Rowley, P.J., Roche, O., Druitt, T.H., Cas, R., 2014. Experimental study of dense pyroclastic density currents using sustained, gas-fluidized granular flows. *Bulletin of Volcanology* 76: DOI 10.1007/s00445-014-0855-1.
- Russell, J.K., Quane, S.L., 2005. Rheology of welding: inversion of field constraints. *Journal of Volcanology and Geothermal Research* 142, 173-191.
- Self, S., 2006. The effects and consequences of very large explosive volcanic eruptions. *Philosophical Transactions of the Royal Society A* 364, 2073-2097.
- Smith, R.L., 1960. Zones and zonal variations in welded ash flow tuffs. *US Geological Survey Professional Paper* 354-F, pp. 149-159.
- Sohn, Y.K., Chough, S.K., 1989. Depositional processes of the Suwolbong tuff ring, Cheju Island (Korea). *Sedimentology* 36, 837-855.
- Sparks, R.S.J., 1976. Grain size variations in ignimbrites and implications for the transport of pyroclastic flows. *Sedimentology* 23, 147-188.
- Sparks, R.S.J., Self, S., Walker, G.P.L., 1973. Products of ignimbrite eruptions. *Geology* 1, 115-118.
- Sparks, R.S.J., Wilson, L., Hulme, G., 1978. Theoretical modeling of the generation, movement, and emplacement of pyroclastic flows by column collapse. *Journal of Geophysical Research* 83, 1729-1739.
- Sulpizio, R., Dellino, P., 2008. Sedimentology, depositional mechanisms and pulsating behaviour of pyroclastic density currents. In: Gottsman, J. and Martí, J. (Eds), *Caldera Volcanism: Analysis, Modelling and Response*. *Developments in Volcanology*, 10. Elsevier, pp. 57-96.
- Sulpizio, R., Dellino, P., Doronzo, D.M., Sarocchi, D., 2014. Pyroclastic density currents: state of the art and perspectives. *Journal of Volcanology and Geothermal Research* 283: 36-65.
- Walker, G.P.L., 1983. Ignimbrite types and ignimbrite problems. *Journal of Volcanology and Geothermal Research* 17, 65-88.
- Willcock, M.A.W., Cas, R.A.F., Giordano, G., Morelli, C., 2013. The eruption, pyroclastic flow behaviour, and caldera in-filling processes of the extremely large volume (> 1290 km<sup>3</sup>), intra- to extra-caldera, Permian Ora (Ignimbrite) Formation, Southern Alps, Italy. *Journal of Volcanology and Geothermal Research* 265, 102-126.
- Wilson, C.J.N., 2001. The 26.5 ka Oruanui eruption, New Zealand: an introduction and overview. *Journal of Volcanology and Geothermal Research* 112, 133-174.

Wilson, C.J.N., Hildreth, W., 1997. The Bishop Tuff: New insights from eruptive stratigraphy. *The Journal of Geology* 105, 407-439.

Wilson, C.J.N., Hildreth, W., 2003. Assembling an ignimbrite: Mechanical and thermal building blocks in the Bishop Tuff, California. *The Journal of Geology* 111, 653-670.

Wilson, C.J.N., Walker, G.P.L., 1982. Ignimbrite depositional facies: the anatomy of a pyroclastic flow. *Journal of the Geological Society of London* 139, 581-592.

Wohletz, K.H., 2006. Fractures in welded tuff. In: Heiken, G. (Ed), *Tuffs, their properties, uses, hidrology, and resources*. Geological Society of America Special Paper 408, 17-31.

Woods, A.W., 1998. Observations and models of volcanic eruptions columns. In: Gilbert, J.S., Sparks, R.S.J. (Eds), *The physics of explosive volcanic eruptions*. Geological Society of London Special Publication 145, pp. 91-114.

Wright, H.M.N., Lesti, C., Cas, R.A.F., Porreca, M., Viramonte, J.G., Folkes, C.B., Giordano, G., 2011. Columnar jointing in vapor-phase-altered, non-welded Cerro Galán ignimbrite, Paycuqui, Argentina. *Bulletin of Volcanology* 73, 1567-1582.

Wright, J.V., 1981. The Rio Caliente ignimbrite: Analysis of a compound intraplinian ignimbrite from a major late Quaternary Mexican eruption. *Bulletin of Volcanology* 44, 189-212.

Figure 1. Geologic map of the study area. Modified from Aguirre-Díaz and López-Martínez (2009) and Aguirre-Díaz (1996). Inset shows the distribution of exposed Huichapan ignimbrite and thickness variations. The top of the Hualtepec intra-caldera dome is the reference point for the distances from the vent discussed in the text. 1- Xithi caldera; 2- Donguinyó caldera; 3- Huichapan caldera; 4- Santa María Macua caldera.

Figure 2. Stratigraphic sections and stratigraphic correlation of the Huichapan ignimbrite with the differentiation between the Lower Huichapan ignimbrite (LHI) and Upper Huichapan ignimbrite (UHI) members. Zones 1, 2, and 3 mentioned in main text are indicated; note how these zones laterally decrease their thicknesses in the LHI. Location of section sites is shown in Fig. 1.

Figure 3. Huichapan ignimbrite outcrop at medial-distal facies in a view to the West (Site 4, Fig. 1) showing diverse cooling joints types in zones 1, 2, and 3. Curved and plumose joints occur in Zone 3. The approximate locations of rock samples are shown at the right side of the photograph.

Figure 4. Photomicrographs of thin sections from the zones 1, 2, and 3 of the LHI (see Fig. 3). a) and (b) show samples of Zone 3 with strong devitrification of glass shards and crystallization in the pore space (white arrows in b). c) Close view of a devitrified fiamme (Fi) showing axiolitic texture; note the quartz (Qtz) at the boundary between the fiamme and the matrix of devitrified glass shards; the sample in (c) is from the Zone 2. d) to h) are photographs of a set of non-devitrified samples showing a wide spectrum of welding

textures, from vitrophyre facies of welding rank 6 (d) to non-welded samples with rank 1 (h); photomicrographs are from the Zone 1.

Figure 5. Lithofacies of the LHI at western outcrops. a) LHI is characterized by monotonous and predominantly poorly-graded mLT and emLT. b) A closer view of the homogenous and structureless mLT; note the cooling joints margins in this photograph. c) close up of the mLT lithofacies; d) vitrophyric eutaxitic variants (vemLT); e) devitrified vitrophyre (devemLT).

Figure 6. Regional stratigraphy and lithofacies variations of the LHI at the northern plateau. The zones 1, 2, and 3 were not developed in this area. An UHI site in the northern plateau is included for reference. See Table 1 for information about lithofacies code usage; a/l/b=ash, lapilli, blocks.

Figure 7. LHI lithofacies at northern outcrops. (a) dbLT defined by a faintly developed concentration of pumice in a laterally and vertically discontinuous horizon, which grades into mLT. (b) mLT that together with the eutaxitic variant (emLT) comprise the majority of LHI lithofacies. (c) Massive lapilli-tuff with well-developed grain fabric (mLTf). (d) The basal mLT layer (lapilli < 2 cm) abruptly grades into mT. The latter abruptly change to a pumice-rich layer (pmLT) showing erosional contact (base of site 27). (e) Same lithofacies as in d without the erosional contact. (e) A basal fine-grained layer (mT) transitionally changes to mLT. (f) some vesicular basalt clast from underlying fluvio-lacustrine deposits are dragged within the pyroclastic deposits.

Figure 8. Main features of the UHI, mostly as a non-welded and non-devitrified ignimbrite. (a) Well-developed, lithic-rich fines-poor pipe within the UHI. (b) The UHI's mLT lithofacies are richer in pumice relatively to the mLT in the LHI. Within the UHI's mLT lithofacies pumice larger than  $-5 \phi$  (including block-sized pumices) are common at all sites. (c) Coarse pumice clasts in a pmBr lithofacies within the UHI.

Figure 9. Simplified composite section of the whole Huichapan ignimbrite. The way in which the LHI changes laterally in welding and devitrification is shown in detail in Figure 2. See discussion section for the interpretation of the ignimbrite.

Figure 10. Schematic representation of the eruptive evolution and distribution of Huichapan ignimbrite-forming PDCs and our large-scale interpretation of deposit distribution after the eruption. Paleotopography is schematic since most of the study area is covered by the Huichapan ignimbrite. The model is subdivided into three representative time slices during the eruption (a, b, and c; see text for discussion). In (d) we show the final assembly of the Huichapan ignimbrite and the emplacement of the post-collapse lavas. We also include which part of the Huichapan ignimbrite has representative logged sites (laterally displaced into the A-A' and B-B' profiles).

Table 1. Lithofacies code abbreviations (adapted from Branney and Kokelaar, 2002; Brown and Branney, 2004).

Table 2. Description and interpretation of the zones 1, 2, and 3 of the LHI.

Table 3. Description and interpretation of selected LHI ignimbrite sites at the northern plateau.

Table 4. Description and interpretation of small volume lithofacies within the Huichapan ignimbrite.

ACCEPTED MANUSCRIPT

Figure 1

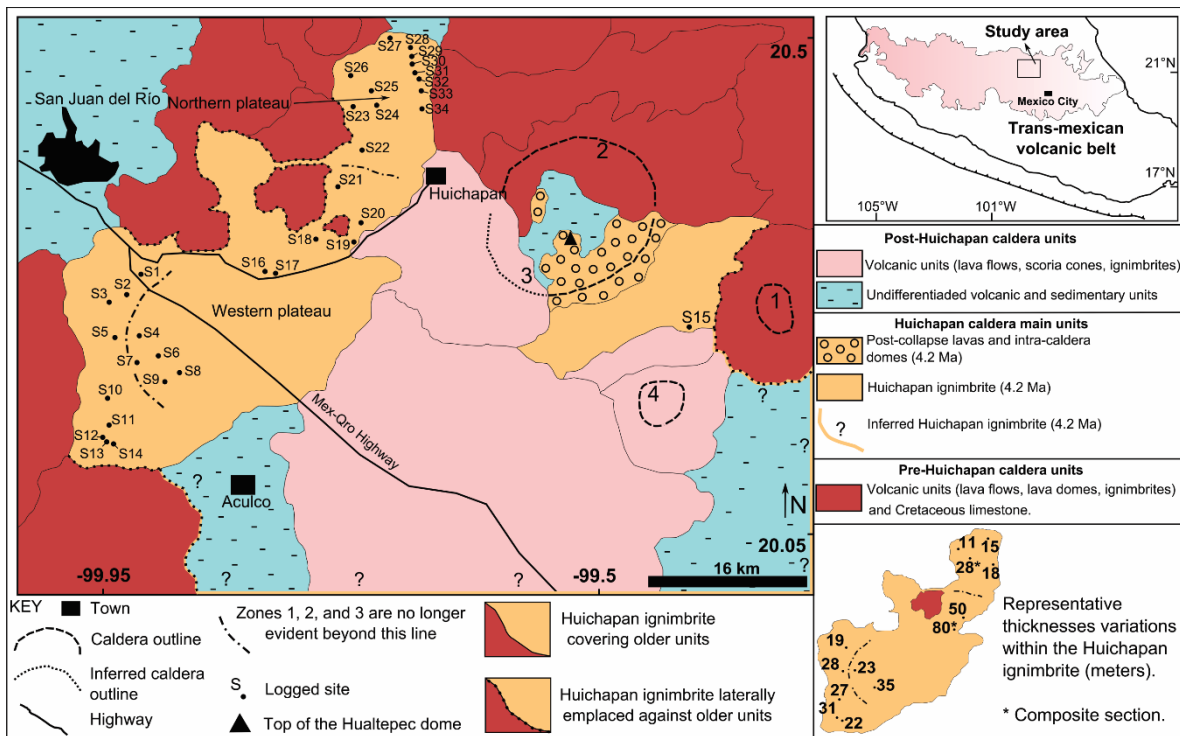


Figure 2

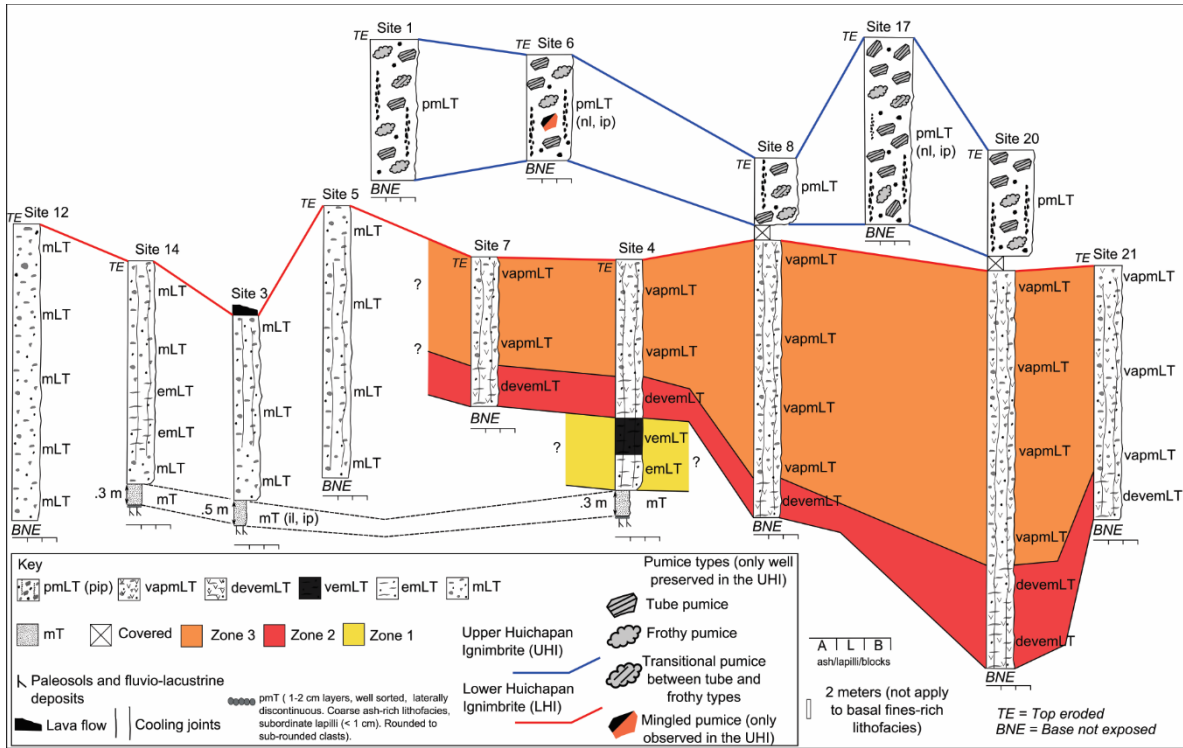


Figure 3



ACCEPTED

Figure 4

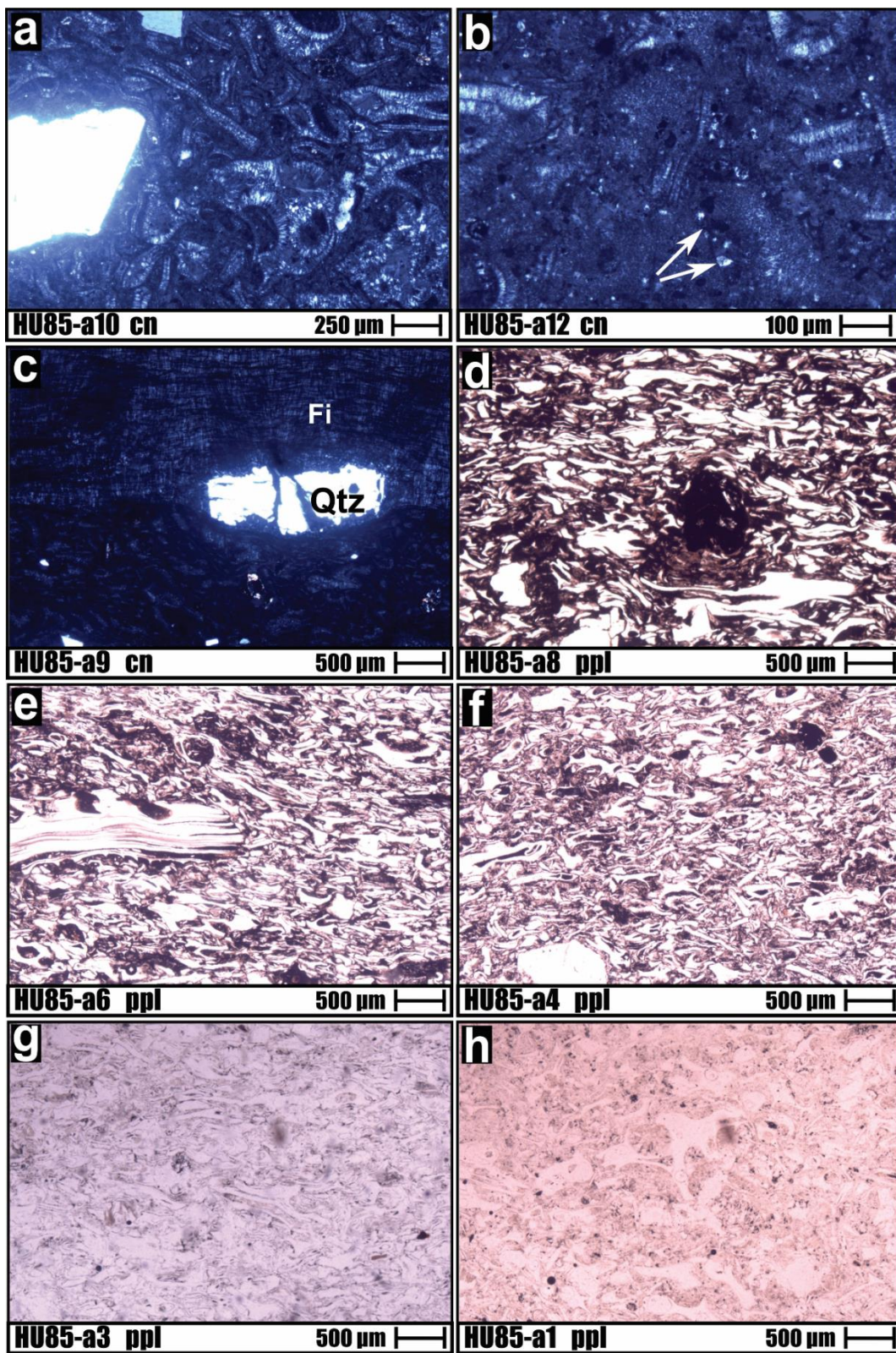




Figure 5

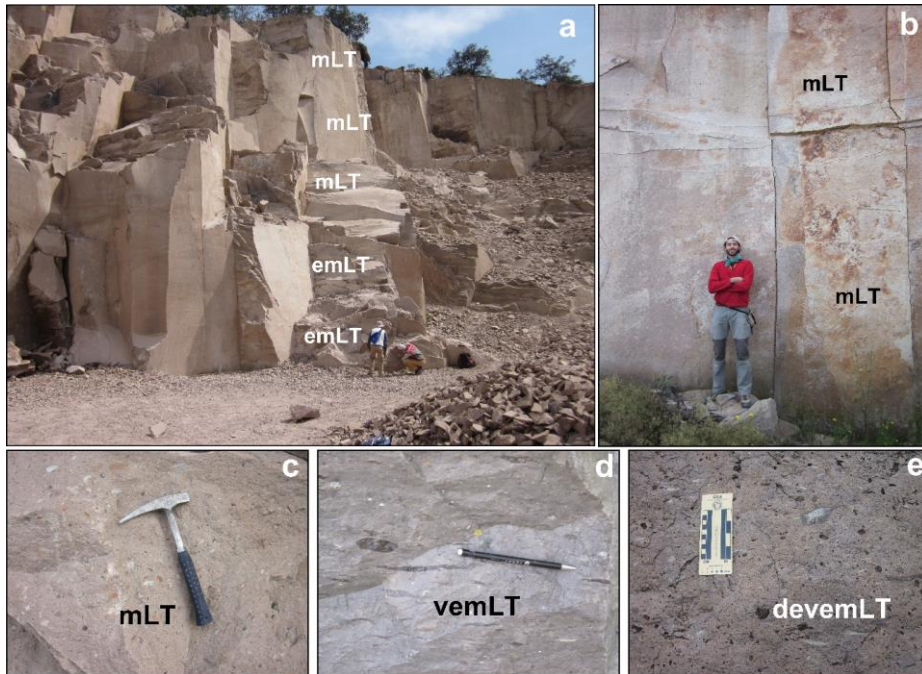




Figure 7

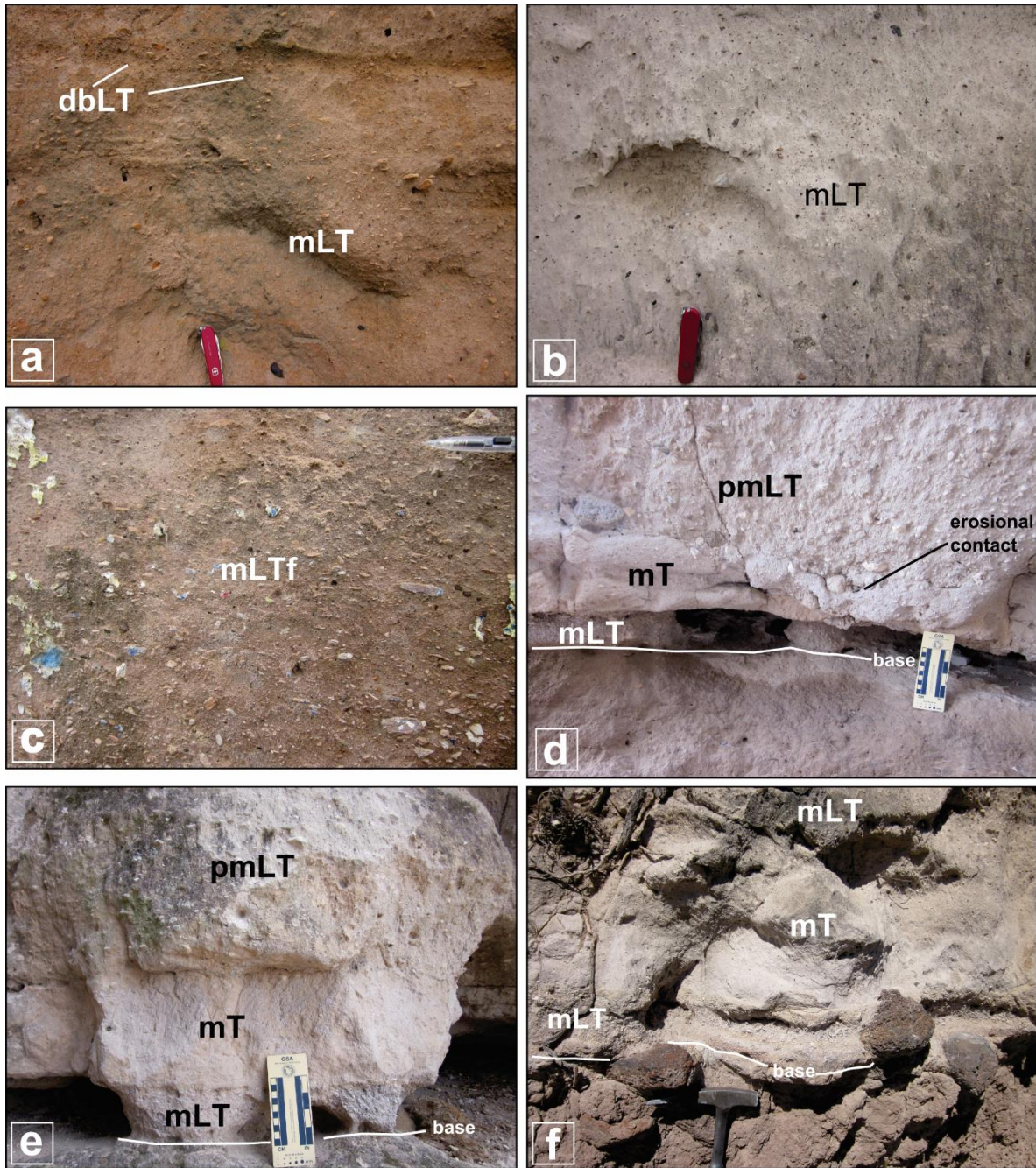
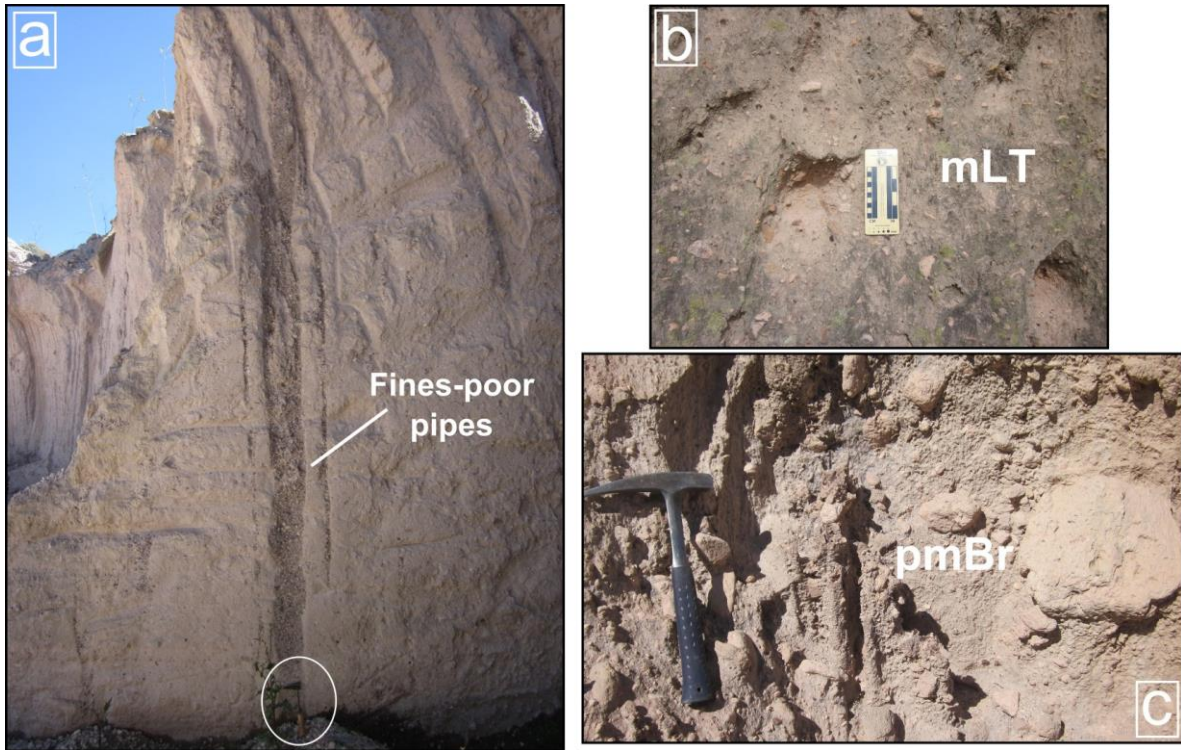
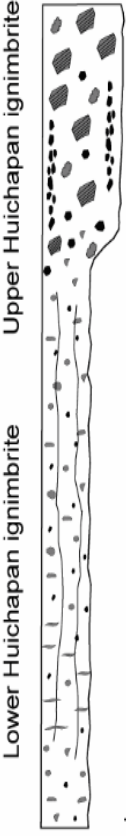


Figure 8



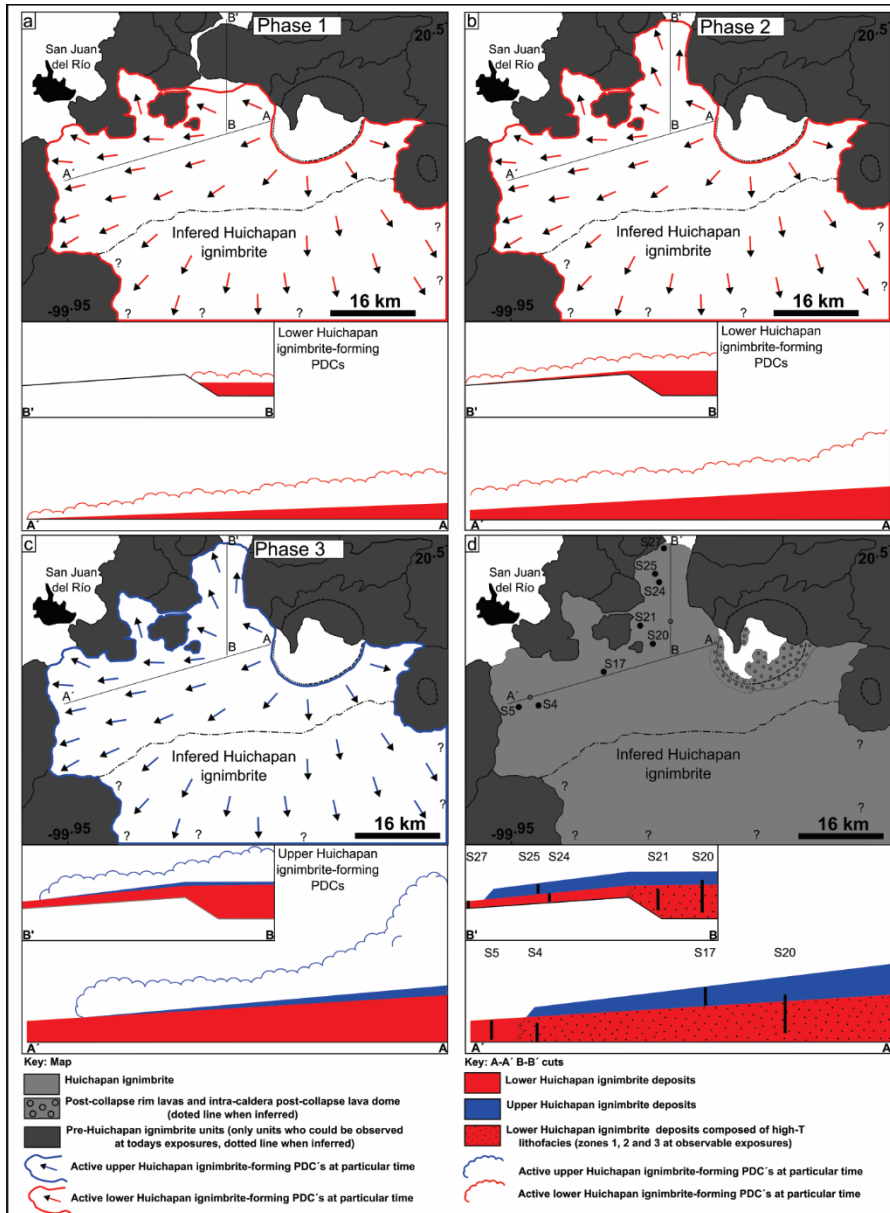
ACCEPTED MANUSCRIPT

Figure 9

	Description	Interpretation
 <p data-bbox="256 346 284 682">Upper Huichapan ignimbrite</p> <p data-bbox="256 766 284 1102">Lower Huichapan ignimbrite</p> <p data-bbox="300 1186 422 1228">A L B ash/lapilli/blocks</p>	<p data-bbox="414 357 885 577">The UHI is non-welded and non-devitrified throughout all its extent. Cooling joints are absent in the UHI. The largest pumice clast reaches between 65 cm and 1 m. The average maximum length for the largest 100 measured lithic clast is 3.13 cm. Lithic-rich elutriation pipes are very common in the UHI.</p> <hr/> <p data-bbox="414 619 885 766">The transition between the UHI and LHI is gradational. Welding, devitrification, and cooling joints not evident upwards. The abundance of lithic-rich elutriation pipes and the size of both lithic and pumice clasts increase upwards.</p> <hr/> <p data-bbox="414 829 885 1102">The LHI varies from non-welded to strongly welded (welding rank 1 to 6), and from non-devitrified to strongly devitrified, including vapor-phase alteration lithofacies. Cooling joints are very common in the LHI and lithic-rich elutriation pipes are almost totally absent. The larger pumice clast within the LHI reaches 12 cm and the average maximum length for the largest 100 measured lithic clasts is 2.01 cm.</p>	<p data-bbox="909 598 1185 882">The Huichapan ignimbrite is a single depositional unit. The differences in granulometry, welding, devitrification, and structures between the UHI and LHI reflect evolving processes during the eruption and in the cooling and depositional histories.</p>

ACCEPTED

Figure 10



**Table 1. Lithofacies code abbreviation.**

Code	Name
mLT	Massive lapilli-tuff
emLT	Eutaxitic massive lapilli-tuff
mBr	Massive breccia
mT	Massive tuff
mpl	Massive pumice lapilli
dbLT	Diffuse-bedded lapilli-tuff
sLT	Stratified lapilli-tuff
dsLT	Diffuse-stratified lapilli-tuff
vemLT	Eutaxitic massive lapilli-tuff vitrophyre
devemLT	Devitrified eutaxitic massive lapilli-tuff
vapmLT	Vapor-phase altered massive lapilli-tuff
(il)	Inverse grading of lithics
(ip)	Inverse grading of pumice
(nl)	Normal grading of lithics
f	Grain fabric
p	Pumice-rich
(pip)	Fines-poor pipes
lensL	Lapilli lenses
—	Lithofacies grading to another within an interval

**Table 2. Description and interpretation of the zones 1, 2, and 3 of the LHI.**

Lithofacies	Description	Interpretation
Zone 1 Lithofacies: mT (massive tuff) mL (massive lapilli-tuff) emLT (eutaxitic massive lapilli-tuff) vemLT (eutaxitic massive lapilli-tuff vitrophyre)	Zone 1 is the lowermost part of the LHI lithofacies, which is exposed only at site 4 (Fig. 2). The first 0.3 m are composed of non-welded mT and mL that gradually change into several meters of emLT and vemLT, gray and black, respectively. Welding grades from rank 1 to rank 6 (Fig. 4). Up to 3.5 meters of vemLT lithofacies was developed in this zone (Fig. 2); the glassy rocks are strongly foliated but do not show structures related to simple shear deformation. Some imbricated fiammes occur in the vemLT. Well-developed vertical columnar jointing is characteristic of Zone 1 (Fig. 3).	The non-welded first centimeters of Zone 1 indicate cooling of PDCs at the contact with the substratum. Glass viscosities were not low enough to rapidly agglutinate and form a basal vitrophyre. In addition, lack of simple shear structures in the vemLT indicates that agglutination was not a predominant process during the formation of the glassy facies. Instead, welding was associated to post-depositional processes. Several meters of eutaxitic ignimbrites with significant proportions of vemLT lithofacies indicate the emplacement of relatively hotter PDCs that were rapidly aggraded, which formed deposits with temperatures exceeding the glass transition for a time-frame that significantly exceeded the relaxation time of glass (e.g., Giordano et al., 2005; Russell and Quane, 2005). Columnar jointing was formed by volumetric contraction and vertical compaction during cooling and welding with joint grow normal to maximum tensile strength (Wohletz, 2006). The fact that cooling joints and welding occurs almost up from the base (Fig. 2) indicates the emplacement of relatively hotter PDCs despite site 4 (type section for Zone 1 deposits) is located at 42 km from the vent. This indicates that currents did not suffer significant cooling during the lateral transport.



<p>Zone 2 Lithofacies: devemLT (devitrified eutaxitic massive lapilli-tuff)</p>	<p>Lithofacies in Zone 2 are devemLT, with strongly developed foliation, including fiammes and flattened glass shards. All the glass (including the fiamme) is strongly devitrified with presence of axiolitic and spherulitic textures (Fig. 4c). The texture of some rocks are similar to that of the vemLT lithofacies of Zone 1, and in cases the rocks show a conchoidal fracture, but fully devitrified. Powder XDR analyses indicate the presence of trydimite and cristobalite. Well-developed, columnar jointing is common in Zone 2 (Fig. 3), sometimes inclined but generally vertical. The transition between zone 1 and zone 2 is abrupt.</p>	<p>Zone 2 deposits represent relatively hotter PDCs that were emplaced immediately after the formation of Zone 1 deposits. The PDC deposits were probably rapidly aggraded, with temperatures exceeding the glass transition for a time-frame that significantly exceeded the relaxation time of glass (e.g., Giordano et al., 2005; Russell and Quane, 2005). This induced the formation of a well-developed eutaxitic texture. After the strong post-depositional welding, the deposits probably kept a high temperature for long time that eventually caused the devitrification of emLT and vemLT lithofacies (e.g., Riehle et al., 1995). Axiolitic and spherulitic textures and the presence of tridymite and cristobalite indicate high-temperature devitrification (Lofgren, 1970, 1971). We interpret columnar jointing in the same way as in Zone 1 but with a likely contribution of devitrification-induced contraction (e.g., Wright et al., 2011).</p>
<p>Zone 3 Lithofacies: vapmLT (vapor-phase altered massive lapilli-tuff)</p>	<p>Lithofacies of Zone 3 are characterized by non-welded rocks, lacking any eutaxitic textures, and are totally devitrified. Lithofacies include vapmLT showing axiolitic and spherulitic textures. Well-developed crystallization of quartz polymorphs within pore spaces is common in Zone 3 (vapor-phase crystallization zone of Smith, 1960; see Fig. 4a,b). Powder XRD analyses indicates the presence of trydimite and cristobalite. Columnar jointing is common and well-developed, grading upwards from straight to curved. Plumose joint sets also occur in Zone 3 (Fig. 3). The transition between zone 2 and zone 3 is gradual.</p>	<p>Axiolitic and spherulitic textures and the presence of tridymite and cristobalite indicate high-temperature devitrification (Lofgren, 1970, 1971). Pore space crystallization indicates precipitation of minerals due to an intense, upward-migrating, vapor-phase activity (Smith, 1960). Cooling joints were formed because of enhanced contraction during devitrification and vapor-phase alteration (Wright et al., 2011). Strongly curved joints and plumose joints in Zone 3 are not close to any inferred paleo-topographic irregularities. In addition, these types of jointing occur in the uppermost part of the LHI, which shows petrographic evidence of vapor-phase alteration, suggesting that these complex jointing patterns are more likely to be an effect of fumarolic processes (Wohletz, 2006).</p>

**Table 3. Description and interpretation of selected LHI ignimbrite sites at the northern plateau.**

Site	Description	Interpretation
Site 26	A basal LT layer (mLT and dsLT lithofacies) abruptly passes into mT lithofacies, the latter transitionally pass into the relatively thick ignimbrite body composed of mLT (nl, ip) lithofacies (Figs. 6 and 7f). The grading of the main ignimbrite body is not of the coarse-tail type.	The basal mLT layers were deposited from the flow fronts of the PDCs (Table 2) and the basal fine-grained layers (mT) record deposition from strongly sheared basal portions of the main PDCs bodies (Table 2). The mLT (ip, nl) is interpreted as recording progressive aggradation of waning currents in a fluid escape-dominated FBZ (e.g., Branney and Kokelaar, 2002). This site can be considered in agreement with the “standard ignimbrite flow unit” Sparks et al. (1973).
Site 27	A basal LT layer (mLT lithofacies) pass in abrupt fashion into a mT lithofacies, the latter pass in abrupt or erosional contact into a pmLT lithofacies (Fig. 7d, e). The outcrop is then followed by the relatively thick ignimbrite body composed of mLT (il, ip) lithofacies, sometimes showing grain fabric (mLTf; Fig. 6).	Same interpretation as in site 26 for the basal LT layer and basal mT lithofacies. The pmLT lithofacies at site 27 are interpreted to record pumice-rich flow fronts of the PDCs embedded in the middle of the deposits because of waxing flow (Table 2). The erosional contact and an overlying mLTf (ip, il) are taken as further evidence of waxing currents at site 27, as the inverse grading of lithics indicates increased flow competence with time and the erosional contact indicates deposition of energetic currents. Deposition occurred from fluid escape-dominated FBZ (mLT) with transitions to granular-flow dominated FB (mLTf).
Site 28	The lithofacies of site 28 are mostly mLT (Fig. 7b), although grain fabric, pumice lenses, and diffuse bedding (mLTf, dbLT, plensL; Fig. 7a, c) are laterally and vertically inconsistent within the overwhelmingly abundant mLT. The granulometry of the deposits continuously change vertically at site 28, from poorly-sorted, relatively thick LT to well-sorted, thin pT layers (Fig. 6). Because of these changes in granulometry, site 28 appears to be the subdivided into three separate ignimbrite bodies when studied alone. Site 28, however, laterally passes to more monotonous, coarsening-upward mLT ignimbrites (Fig. 6).	Laterally discontinuous grain fabric, pumice lenses, and bedding (pmTf, dbLT, mLTf, plensL) are interpreted to record some unsteadiness and shearing in the FBZ, probably in transitions between fluid escape- and granular flow-dominated FBZ, whereas more monotonous portions of the deposit (mLT, mLT (ip)) record conditions in a fluid escape-dominated FBZ. Continuously vertically changes in grading, bedding, fabric, and grain size at site 28 are interpreted to record deposition of surging currents. The fact that site 28 laterally passes into more monotonous outcrops is an effect of spatially evolving primary sedimentary structures within the ignimbrite’s architecture (e.g., Brown and Branney, 2013) rather than the occurrence of three separate ignimbrite bodies at this site. The lateral evolving primary sedimentary structure are interpreted to record non-uniform FBZ processes trough time and space.

Site 29-33	The lithofacies are overwhelmingly composed by monotonous mLT, at some of the best-preserved sites (29, 30, and 32) the size of both lithic and pumice clasts increase upwards.	The deposits of the LHI in these sites record deposition from quasy-steady, density-stratified high-concentration currents in a fluid-escape dominated FBZ. At some sites, some unsteadiness is recorded because of the coarsening-upward succession, which indicates that the size of both lithic and pumice clast reaching the FBZ increased with time. This may be due to a size increase of both lithic and pumice clast at the vent and/or increased flow competence.
Site 35	Fine-grained deposits (mT) vertically pass into mLT; at site 35, a discontinuous pumice rich-layer (pmBr) is embedded between more fine-grained layers (mLT, mLTf); all these lithofacies pass upwards into poorly-sorted mLT – emLT lithofacies (Fig. 6).	The basal fine-grained portions of the deposits may record kinematic sieving processes during the first stages of deposition at site 35 (Table 2), and the discontinuous pumice rich-layers (pmBr) record the passage of waxing currents (Table 2). The overlying monotonous and poorly graded lithofacies (mLT, emLT) record deposition of quasy-steady PDCs. Deposition at site 35 occurred during fluid escape-dominated FBZ (e.g., mLT, pmBr) with transitions to granular flow-dominated FBZ (mLTf). The deposition history at site 35 could be defined as waxing and then quasy-steady PDCs.

Table 4. Description and interpretation of small volume lithofacies within the Huichapan ignimbrite

Lithofacies	Description	Interpretation	Notes
Pumice-rich layers. Lithofacies: pmLT; pmBr Occurrence: LHI	<i>Lithology:</i> 20-30 cm thick; angular to sub-rounded pumice clast (10-40 modal %); the breccia facies (pmBr) are clast-supported and dominated by angular to sub-angular clast; pmLT are matrix supported and have common occurrence of sub-rounded and rounded pumice; the lithofacies are non-welded, poorly sorted and poor in crystals and lithics (<1% each); Pumice clasts up to 12 cm. <i>Structure:</i> Massive and non-graded. <i>Geometry:</i> sub-horizontal, laterally discontinuous layers; these lithofacies pass laterally and vertically in abrupt or erosional fashion into more fine-grained lithofacies (mT, mLT, mLTf, this last one always above the pumice-rich layers).	The pumice-rich layers are interpreted as recording segregated pumice at the leading margin of the PDCs main body that, before overpassing, were then trapped within the deposit because of waxing flow (Branney and Kokelaar, 2002). Because of that, the pumice-rich layers are embedded between more fine-grained lithofacies; Deposition occurred in a fluid-escape dominated FBZ of high-concentration PDCs; close association with overriding mLTf indicates that after the formation of the pumice-rich layers deposition is transitional between fluid escape- and granular flow-dominated FBZ.	Photographs of pumice-rich layers (sites 34 and 27) are presented in the supplementary material 2. These lithofacies are presented in Fig.6 (see sites 34 and 27).
Fine-grained basal layers. Lithofacies: mT; mT (il, ip) Occurrence: LHI	<i>Lithology:</i> sub-angular to sub-rounded pumice clast (<2 cm); pumice clast is <5%; non-welded; lithic- and crystal-poor (each <1%); well sorted white ash-rich tuff layers. <i>Structure:</i> massive; non-graded to inversely graded. <i>Geometry:</i> these lithofacies occur at the lower portion of the ignimbrite's main body; in most cases are less than 1 m thick and pass abruptly or transitionally into mLT or pmLT lithofacies; the fine-grained basal layers occur only at some sites but laterally disappear between neighboring outcrops (see Fig. 6, sites 26-30).	Segregation by kinematic sieving (e.g., Legros, 2002) within strongly shearing basal portions of PDCs main body; the inverse grading record continuously less effective kinematic sieving with time during progressive aggradation; massive nature suggest deposition of high-concentration PDCs in a fluid-escape dominated FBZ; the fact that these lithofacies are not well developed at some sites indicates that kinematic sieving did not occur at some locations; the fine-grained basal layers are not a stratigraphic horizon, instead these lithofacies record particular segregation processes that may or may not occur during the first stages of deposition at particular locations.	Images of fine-grained basal layers are presented in Fig.7d-f. These fine-grained basal layers are referred by some authors as "2a layers" (Sparks et al., 1973; Cas and Wright, 1987; Freundt et al., 2000).

<p>Basal lapilli-tuff layers. Lithofacies: mLT; mLTf, dsLT Occurrence: LHI</p>	<p><i>Lithology:</i> massive and moderately well sorted; lapilli-tuff lithofacies with lack of pumice coarser than 2 cm (relatively fine-grained LT compared with the main ignimbrite); lithic- and crystal-poor (each &lt;1%); non-welded; matrix- to clast-supported; sub-angular to rounded pumice; 5-8 cm thick. <i>Structure:</i> predominantly massive passing to diffuse stratified; poorly graded; sometimes with faintly developed grain fabric. <i>Geometry:</i> these lithofacies do not show significant regional grain size and thickness variations; substratum-derived cobble-sized basalt clasts are drag between these lithofacies; the basal lapilli-tuff layers abruptly pass into mT and mLT of the main ignimbrite body.</p>	<p>The sub-rounded and rounded clast record abrasion during deposition of PDCs (e.g., Manga et al., 2011); we interpret the basal lapilli-tuff layers as being deposited from the flow fronts of PDCs; these flow fronts may develop because of air ingestion, burning of vegetation and/or ingestion of substrate water (Wilson and Walker., 1982): Nevertheless, predominantly massive character suggests that high-particle concentration and turbulence inhibition were predominant even to PDCs fronts with FBZ processes dominated by fluid-escape (mLT) with transitions to traction-dominated (dsLT) and granular flow (mLTf).</p>	<p>These lithofacies are traced between sites 26-28 in Fig 6.</p>
<p>Pumice concentration zones: Lithofacies: pmBr Occurrence: UHI</p>	<p><i>Lithology:</i> Sub-angular to rounded pumice (both lapilli- and block-sized, 10-40 modal %); predominantly clast-supported; poorly sorted; lithic- and crystal-poor (each &lt;1%). <i>Structure:</i> massive and non-graded. <i>Geometry:</i> sub-circular to curved pumice concentration zones; these lithofacies pass laterally and vertically in abrupt fashion into mLT and mLT (pip); these pumice concentration zones do not occur at ignimbrite's distal margins or in channelized portions of the deposits, instead, they occur within internal portions of a laterally continuous extensive ignimbrite sheet.</p>	<p>Segregated and concentrated pumice clasts by the effect of hindered settling and upward-migrating fluid escape; the pumice clasts concentrations were "freeze" within the deposits before overpassing because of very high deposition rate during rapid progressive aggradation of high-concentration PDCs in a fluid escape-dominated FBZ.</p>	<p>These lithofacies are shown in the supplementary material 2. These lithofacies have been observed at site 17.</p>

<p>Stratified lapilli-tuff bedforms: Lithofacies: sLT, dsLT Occurrence: UHI</p>	<p><i>Lithology:</i> sub-rounded to well-rounded pumice lapilli; non-welded; predominantly matrix-supported; poorly sorted; lithic- and crystal-poor (each &lt;1%); block-sized pumices are absent within these lithofacies. <i>Structure:</i> parallel to sub-parallel strata 1-10 cm thick; lithofacies grade laterally between sLT into dsLT; sometimes well-rounded pumice are concentrated in parallel to stratification layers. <i>Geometry:</i> sub-horizontal to curved bedforms; these lithofacies pass laterally and vertically in abrupt fashion into thick mLT and mLT (pip) deposits; the bedforms pinches out laterally; these bedforms have rare occurrence within a massive and laterally continuous extensive ignimbrite sheet; these lithofacies have been observed at 28 km from the vent.</p>	<p>Stratification suggests deposition of a traction dominated-FBZ; the sub-rounded and rounded pumice clasts record abrasion during deposition of PDCs (e.g., Manga et al., 2011); since these lithofacies occur at 28 km from the vent it is unlikely that they represent single-surge dilute currents; the fact that the bedforms develop erratically within the outcrops passing both laterally and vertically into large and monotonous massive ignimbrite indicates the formation by a particular and localized processes; we interpreted these bedforms as being develop from turbulent eddies, which locally affect the deposition processes within largely sustained high-concentration PDCs; the turbulent eddies induce local formation of traction processes, forming the sLT passing into dsLT as the turbulent eddies loss energy.</p>	<p>These lithofacies are shown in the supplementary material 1 and have been observed at sites 16 and 17. Stratified deposits enclosed between thick mLT have been reported by Fisher (1979) and interpreted to record dilute currents segregated from the top of concentrated PDCs. Branney and Kokelaar (2002) argue that these kinds of structures may represent temporary fluctuations of FBZ processes within the deposition of a single and sustained PDC.</p>
---	---	---	--

## HIGHLIGHTS VOLGEO 2017-52-R1

- The voluminous (69 km<sup>3</sup> DRE), 4.2 Ma Huichapan ignimbrite, at the Central Mexican Volcanic Belt, has been described on the basis of field relations, stratigraphy and lithofacies associations.
- Depositional processes have been interpreted based on the superb massive exposures of the Huichapan outflow bed and textural changes.
- The Huichapan ignimbrite have been formed from uninterrupted and largely sustained, dense pyroclastic fountains with high mass-flow rate, promoting high mobility of the pyroclastic density currents with a minimum coverage of 2460 km<sup>3</sup>.
- Quasi-steady deposition of dense pyroclastic density currents is the predominant depositional process; complexities within the ignimbrite architecture suggest the presence of waxing and waning stages.
- Welding and vapor-phase alteration variations within the ignimbrite are related to both post-depositional cooling processes and height changes in the pyroclastic fountains.

ACCEPTED MANUSCRIPT